Dishevelled interacts with the DIX domain polymerization interface of Axin to interfere with its function in down-regulating β-catenin

Marc Fiedler, Carolina Mendoza-Topaz, Trevor J. Rutherford, Juliusz Mieszczanek, and Mariann Bienz[1]

Medical Research Council Laboratory of Molecular Biology, Cambridge CB2 0QH, United Kingdom

Edited* by Roeland Nusse, Stanford University School of Medicine, Stanford, CA, and approved December 21, 2010 (received for review November 15, 2010)

Wnt/β-catenin signaling controls numerous steps in normal animal development and can also cause cancer if inappropriately activated. In the absence of Wnt, β-catenin is targeted continuously for proteasomal degradation by the Axin destruction complex, whose activity is blocked upon Wnt stimulation by Dishevelled, which recruits Axin to the plasma membrane and assembles it into a signalosome. This key event during Wnt signal transduction depends on dynamic head-to-tail polymerization by the DIX domain of Dishevelled. Here, we use rescue assays in *Drosophila* tissues and functional assays in human cells to show that polymerization-blocking mutations in the DIX domain of Axin disable its effector function in down-regulating Armadillo/β-catenin and its response to Dishevelled during Wnt signaling. Intriguingly, NMR spectroscopy revealed that the purified DIX domains of the two proteins interact with each other directly through their polymerization interfaces, whereby the same residues mediate both homo- and heterotypic interactions. This result implies that Dishevelled has the potential to act as a "natural" dominant-negative, binding to the polymerization interface of Axin's DIX domain to interfere with its self-assembly, thereby blocking its effector function.

The Wnt effector β-catenin is a transcriptional coactivator that controls numerous cell fates in normal animal development and tissue homeostasis, and it can also mutate to a potent oncogene (1, 2). In the absence of a Wnt signal, β-catenin binds to the adenomatous polyposis coli (APC) tumor suppressor and is thus recruited to the Axin destruction complex, which promotes its phosphorylation by casein kinase 1 (CK1) and glycogen synthase kinase 3β (GSK3β) to target it for proteasomal degradation. Phosphorylation of β-catenin depends critically on a scaffolding effect afforded by Axin, which binds simultaneously to GSK3β and its β-catenin substrate through a central domain (3, 4). Upon Wnt stimulation, Dishevelled (Dsh in flies, or Dvl in mammals) interacts with Axin to recruit it to the plasma membrane (PM) (5), where Dvl assembles a stable signalosome in which it stimulates the phosphorylation of multiple motifs in the cytoplasmic tail of the LRP6 coreceptor (6–8). One of these phosphorylated motifs (phospho-PPPSPXS/T) acts as a direct competitive inhibitor of GSK3β (9, 10), blocking its activity toward β-catenin, thus allowing unphosphorylated β-catenin to accumulate and operate a transcriptional switch in the nucleus—the key functional output of Wnt/β-catenin signaling in normal development and in disease (1, 2).

Axin contains two structured and conserved domains at its termini that mediate additional functional interactions: through its N-terminal RGS domain, it binds directly to APC (11, 12), whereas its C terminus contains a DIX domain that mediates Axin homodimerization (13–15) and that is also required but not sufficient for Axin's interaction with Dsh/Dvl (16–18). The DIX domain is found only in two other protein families—namely in Dsh/Dvl proteins (see *Results*) and in Ccd1, which regulates a noncanonical Wnt signaling branch (19). A remarkable molecular property of the Dvl DIX domain is its ability to self-associate ("polymerize") dynamically and reversibly in vitro and in vivo, which is critical for the signaling activity for Dvl2—likely because Dvl2 polymerization generates a fluid interaction platform with a high local concentration of ligand-binding sites, which increases the avidity of Dvl2 for its low-affinity ligands (20, 21). Consistent with this notion, the crystal structure of the Axin DIX domain (to be called DAX, to distinguish it from Dvl DIX) revealed a head-to-tail filament, with close molecular contacts between key "head" and "tail" residues in the DAX–DAX interface (Fig. 1 *A* and *B*); the functional relevance of the corresponding DIX residues for the signaling activity of Dvl2 was demonstrated by their mutations, which block DIX polymerization in vitro and Dvl2 self-assembly in vivo (20) and which attenuate signalosome assembly at the PM and phosphorylation of the LRP6 cytoplasmic tail (6, 8). Whether the DAX-mediated polymerization of Axin is required for its effector function, and/or for its interaction with Dsh/Dvl, has not been determined. Indeed, it remains an open question how the two proteins interact at the molecular level and whether Axin is inhibited directly by Dsh/Dvl.

Here, we generate point mutations in the DAX–DAX interaction surface that block its DAX polymerization, and we use rescue assays in *Drosophila axin* null mutant tissues and functional assays in human cells, to show that the ability of this domain to polymerize is critical for Axin's effector function in down-regulating Armadillo/β-catenin as well as for its response to Dsh/Dvl2. NMR spectroscopy revealed that the same head and tail residues that engage in DAX homopolymerization also mediate the direct interaction with the polymerization interface of Dvl2 DIX. An interesting implication of these findings is that Dvl proteins could use their DIX domains not only to assemble signalosomes, but also to interfere with the effector function of Axin, by competing with its self-association. Therefore, by virtue of their DIX domain, Dvl proteins have the potential to behave as natural "dominant-negatives" of Axin.

Results

We used the X-ray structure of the DAX filament (20) to design point mutations in head (M3, M4) and tail residues (M2, M5) that mediate close DAX–DAX contacts in the polymerization interface (Fig. 1 *A* and *B*), for functional tests in vitro and in vivo. Multiangle laser light scattering (MALLS) of purified wild-type (wt) and mutant domains revealed that wt DAX forms large self-assemblies, with an apparent molecular mass of 98.3 kDa (roughly corresponding to an octamer), whereas mutant DAX domains exhibit far lower molecular masses, consistent with monomers (Fig. 1*C*), as expected from the behavior of their DIX mutant counterparts (20). Consistent with this result, although full-length Axin (tagged with green fluorescent protein, GFP) forms striking

Author contributions: M.B. designed research; M.F., C.M.-T., T.J.R., and J.M. performed research; M.F., C.M.-T., T.J.R., and J.M. analyzed data; and M.B. wrote the paper.

The authors declare no conflict of interest.

*This Direct Submission article had a prearranged editor.

[1]To whom correspondence should be addressed. E-mail: mb2@mrc-lmb.cam.ac.uk.

This article contains supporting information online at www.pnas.org/lookup/suppl/doi:10.1073/pnas.1017063108/-/DCSupplemental.

CELL BIOLOGY

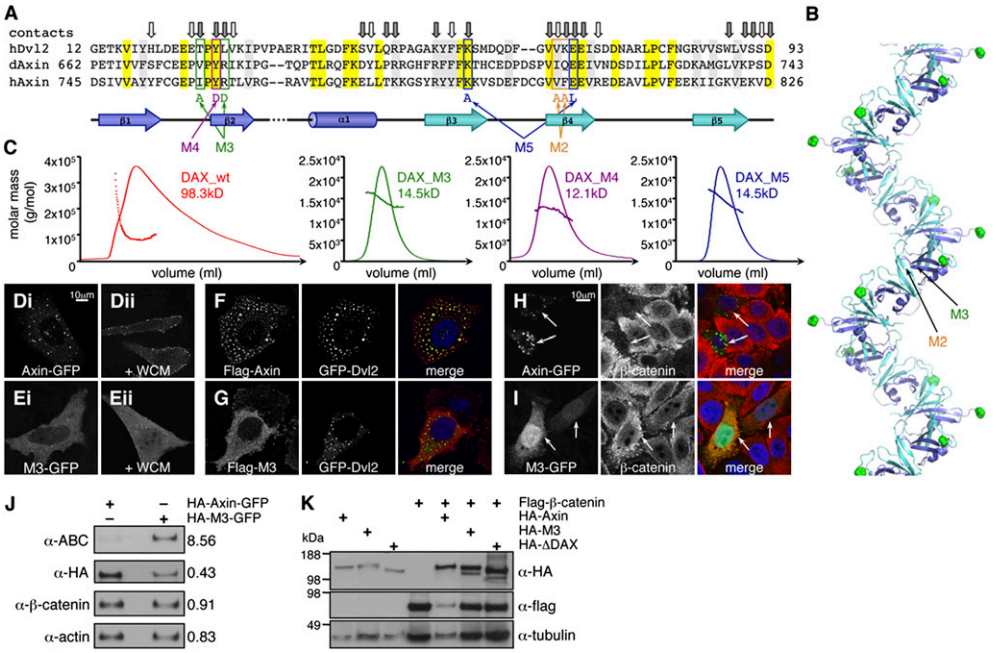

Fig. 1. Polymerization-blocking DAX mutations attenuate Axin's response to Dvl and its effector function in down-regulating β-catenin in human cells. (*A*) Alignment of amino acid sequences of DAX (from human and *Drosophila* Axin) with DIX (from human Dvl2), with secondary structure elements of head and tail regions underneath (blue, head; turquoise, tail) and polymerization-blocking DAX mutations indicated. Invariant (yellow) and semiconserved (gray) residues are shaded; surface residues engaged in close DAX–DAX interactions (20) are marked by arrows (with the closest interactions in gray). (*B*) Ribbon representation of DAX filament, with head regions of individual DAX monomers in blue, tail regions in turquoise, and N-termini marked by green spheres, and positions of M2 and M3 indicated (in one DAX–DAX interface). (*C*) MALLS of purified wt and mutant DAX domains. (*D*–*G*) Confocal images of fixed HeLa cells, expressing wt or M3 mutant Axin-GFP (plus recruitment mixture; refs. 6 and 22) upon exposure to control or WCM (for 2 h) (*D* and *E*), or coexpressing wt or M3 mutant Flag-Axin with GFP-Dvl2, as indicated (*F* and *G*). (*H* and *I*) Confocal images of fixed SW480 cells, expressing wt or M3 mutant Axin-GFP (individual transfected cells indicated by arrows), stained for β-catenin (red). (*J*) Western blot analysis of total lysates from FACS-sorted SW480 cells expressing low levels of wt or M3 mutant HA-Axin-GFP, probed with antibodies as indicated [active β-catenin (ABC)]; numbers indicate levels at right relative to left (set to 1) as measured by densitometry. (*K*) HeLa cells cotransfected with Flag-β-catenin plus wt or mutant HA-Axin-GFP, as indicated; equal amounts of total protein were loaded in each lane; note that HA-M3-GFP is as inactive in down-regulating Flag-β-catenin as an Axin deletion mutant lacking its entire DAX domain (HA-ΔDAX).

dynamic puncta in transfected HeLa cells (21) (Fig. 1*Di*), M4-GFP and M2-GFP are mostly diffuse, forming only residual puncta (22), whereas M3-GFP is entirely diffuse (Fig. 1*Ei*) at the low expression levels used in this study (*Materials and Methods*). These DAX mutants therefore attenuate, or block, the self-association of DAX in vitro and full-length Axin in cells.

Polymerization-Blocking DAX Mutations Attenuate Axin's Response to Dvl and Its Effector Function in Down-Regulating β-Catenin. To test the Dvl response of the polymerization-defective Axin mutants, we conducted membrane-recruitment assays in transfected HeLa cells upon exposure to Wnt3a-conditioned medium (WCM): As previously shown (6, 22), virtually all Axin-GFP puncta translocate to the PM within 30–60 min of Wnt3a stimulation (Fig. 1*Dii*). In contrast, we observe no Wnt3a-induced PM association of M3-GFP, whose diffuse cytoplasmic distribution remains essentially unchanged upon Wnt3a stimulation (Fig. 1*Eii*), suggesting that this mutant fails to interact with Dvl. In support of this result, whereas wt Flag-Axin colocalizes precisely with GFP-Dvl2 puncta upon coexpression (Fig. 1*F*), reflecting its recruitment into cytoplasmic Dvl2 signalosomes (22), Flag-M3 shows only residual recruitment into the GFP-Dvl2 puncta (Fig. 1*G*). The same was observed in SW480 cells for Flag-M3 and Flag-M2 (see next paragraph), confirming that the Dvl response of polymerization-defective Axin mutants is also attenuated in these colorectal cancer cells.

SW480 cells are mutant for *APC* and, thus, exhibit high levels of unphosphorylated β-catenin (23), which can be exploited for effector function tests of Axin proteins because these proteins are capable of down-regulating the high β-catenin levels upon overexpression (11, 12). As expected from these earlier studies, we find that every SW480 cell that expresses punctate Axin-GFP shows low β-catenin levels (Fig. 1*H*). In contrast, M3-GFP is diffuse and fails to reduce the β-catenin levels (Fig. 1*I*). We also used Western blot analysis to confirm that the activity of M3-GFP in down-regulating β-catenin is impaired compared with Axin-GFP in transfected SW480 cells, after fluorescence-activated cell sorting (FACS), to enrich for propidium iodide-negative (i.e., alive) cells with low GFP expression levels (i.e., 10–100× above background), discarding the cells exhibiting high GFP expression levels (i.e., 100–1,000× above background, corresponding to more than half of all GFP-positive cells; Fig. 1*J*), or in transfected HeLa cells that coexpress Flag-β-catenin and M3-GFP (Fig. 1*K*). Our results indicate that Axin relies on DAX-dependent polymerization for its effector function in down-regulating β-catenin.

Polymerization-Defective Axin Mutants Exhibit Diminished Effector Function in *axin* Mutant *Drosophila* Tissues. To test this more rigorously—namely in a physiological setting and in the absence of endogenous Axin—we generated M2, M3, and M4 mutants of *Drosophila* Axin-GFP (5), and used these for rescue assays in *axin* null mutant *Drosophila* embryos. As previously described (5), we observe Axin-GFP puncta at two distinct subcellular localizations upon moderate expression (mediated by *arm.GAL4*) throughout the embryonic epidermis: in cells between the Wingless (Wg) expression zones, Axin-GFP puncta are cytoplasmic (Fig. 2*A*, brackets), whereas within the Wg zones (Fig. 2*A*, arrows), these puncta are associated with the PM (Fig. 2*A*, arrowheads),

reflecting Dsh-dependent PM recruitment. In contrast, if we express polymerization-defective Axin mutants, these are mostly diffuse, and we only observe rare PM-associated puncta in each case (Fig. 2 *B* and *C*), indicating that their interaction with Dsh is disabled, agreeing with our results in human cells.

Next, we tested the polymerization-defective Axin mutants for their ability to rescue *axin* null mutant embryos. Fully developed wt embryos exhibit denticle belts (reflecting Axin effector function; Fig. 2*D*, brackets), alternating with segments of naked cuticle (reflecting Axin inhibition by Wg and Dsh; Fig. 2*D*, arrows), whereas *axin* null mutants show entirely naked cuticles (24) (Fig. 2*E*). Overexpression of wt Axin-GFP with *arm.GAL4* restores complete and normal denticle belts (plus often also ectopic denticles) in 80% of the *axin* mutant embryos (213/267; Fig. 2 *F* and *H*), but this rescue activity is clearly reduced in the case of M4 and M2, which restore complete denticle belts in only 36% (155/437) and 59% (94/158) of the *axin* mutants, respectively (Fig. 2 *G* and *H*; for embryonic expression levels of wt and mutant Axin-GFP, see Fig. 2*I*). If we use *Antp.GAL4* for these rescue assays (to generate low expression levels), we observe robust rescue activity of M3 in only 10% of the *axin* mutants, whereas Axin-GFP produces robust rescue activity in 32% of the mutants (Fig. S1). As expected from these results, we observe wide-spread derepression of the Wg target gene *engrailed* (*en*) in the embryonic epidermis of *axin* null mutants that express M3 or M2, as in the *axin* mutants themselves (24), whereas Axin-GFP-expressing *axin* mutants show the normal narrow stripes of *en* expression (Fig. S2*A*). Likewise, the cytoplasmic Armadillo levels remain high in M3- or M2-expressing *axin* mutants (except for the two parasegments in which *Antp.GAL4* mediates the highest expression levels; see brackets in Fig. S2 *B* and *C*), but are reduced to background levels by midembryogenesis by wt Axin-GFP (Fig. S2*B*). Thus, Axin relies on DAX-dependent polymerization for its effector function in the embryonic epidermis—i.e., to reduce the levels of Armadillo and to antagonize Wg-dependent gene expression and phenotypic outputs.

We also tested the function of wt and mutant Axin-GFP in *axin* null mutant wing disk clones in which ectopic activation of the Wingless target gene *senseless* (*sens*) (expressed on either side of the Wg expression stripe along the prospective wing margin; Fig. 3*A*) is observed cell-autonomously, as a result of the ectopic Armadillo stabilization in the absence of Axin function (25) (Fig. 3*B*). We found that wt Axin-GFP down-regulates *sens* expression efficiently within *axin* mutant clones (Fig. 3*C*, boxed) as well as outside these clones along the wing margin where *sens* is normally activated by Wg (Fig. 3*C*, arrowhead), whereas M2 fails to do so within and outside the mutant clones (Fig. 3*D*, boxed and arrowhead). This finding confirms our results in the embryo that the polymerization-defective mutants are less active than wt Axin with regard to their effector function in antagonizing Wg and Armadillo signaling outputs.

Polymerization Surfaces of DAX and DIX Participate in Direct Heterotypic Interactions. Kishida et al. (16) reported direct physical interactions between bacterially expressed DIX domain fragments plus extensive flanking sequences from Dvl1 and Axin, which was recently confirmed (26). We therefore wondered whether a failure in direct binding could account for the observed defects of our DAX mutants in their response to Dsh/Dvl. We note that previous pulldown assays failed to detect a direct interaction between the minimal DIX and DAX domains themselves (16, 22); however, these negative results may have been due to a low affinity between the two domains: We have used analytical ultracentrifugation to estimate a K_d of 5–20 μM for DIX self-association (20), similarly to the DAX self-interaction that was reported to be weak (15). The heterotypic interaction between the two domains appears even weaker (see *Results*), which explains why this interaction tends to be undetectable by standard pulldown assays or coimmunoprecipitation.

We thus used NMR spectroscopy as a highly sensitive probe for intermolecular interactions in solution to ask whether we could detect direct binding between the purified minimal DIX and DAX domains themselves. To avoid complications with polymerization of the purified domains at the high concentrations required for NMR spectroscopy (27), we acquired ^{1}H-^{15}N heteronuclear single-quantum correlation (HSQC) spectra of ^{15}N-labeled DAX mutants, from which we selected the head mutant DAX_M3 for assignments of resonances and further analysis. Incubation of ^{15}N-DAX_M3 with wt DAX revealed noticeable chemical shift perturbations, or exchange broadening (referred to as "line broadening" below) of numerous resonances, which correspond to residues in the polymerization interface of the head-to-tail filament in the crystal structure (20). Importantly, we did not

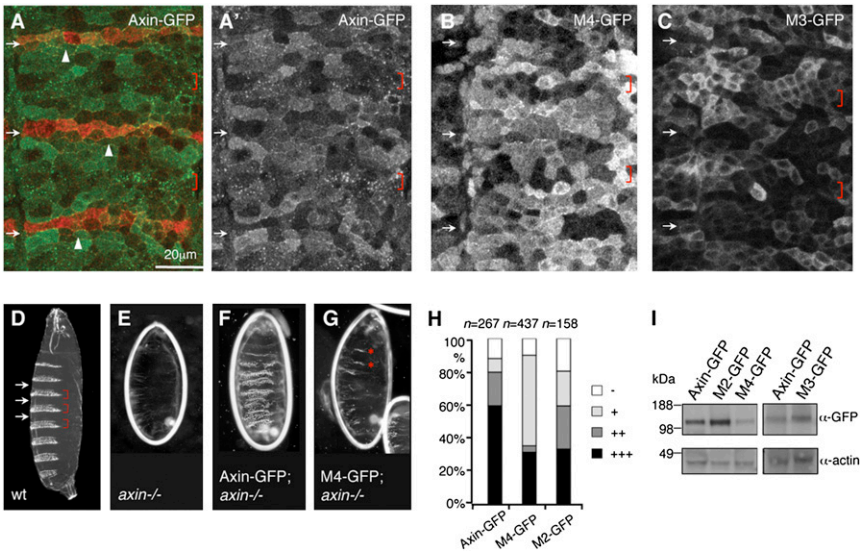

Fig. 2. Attenuated rescue activity of polymerization-defective Axin mutants in *axin* null mutant *Drosophila* embryos. (*A*–*C*) Confocal sections of the lateral epidermis of ≈6-h-old embryos, after fixation and staining with α-Wg antibody (red), expressing wt (green) (*A*) or mutant Axin-GFP in the embryonic epidermis, as indicated (*B* and *C*) (with *arm.GAL4*, which mediates somewhat patchy expression, with nonexpressing cells interspersed between GFP-expressing cells; only the green channel is shown for *A*′, *B*, and *C*). Arrowheads point to Dsh-dependent PM association of Axin puncta in the Wg-expressing zones (marked by arrows in *A*–*C*); brackets indicate zones with cytoplasmic Axin puncta, likely reflecting the Axin destruction complex (because they also contain APC; ref. 5). (*D*–*G*) Dark-field views of the ventral epidermis of fully developed wt or *axin* null mutant embryos, $^{+/-}$ overexpression of wt or M4 mutant Axin-GFP, as indicated. Arrows point to naked zones (i.e., the output of embryonic Wg signaling in the cuticle), and brackets indicate the denticle belts (i.e., the output of Axin effector function). The majority of Axin-expressing *axin* mutants show normal denticle belts plus ectopic denticles (*F*) (5), whereas most M4-expressing mutants show merely rudimentary denticle belts (*G*, asterisks). (*H*) Semiquantitative analysis of rescue activities of wt and mutant Axin-GFP. +++, normal denticle belts with ectopic denticles interspersed; ++, normal denticle belts; +, <4 rudimentary denticle belts; –, naked (no rescue activity). (*I*) Western blots (from two independent experiments) of total embryonic extracts after expression of wt or mutant Axin-GFP.

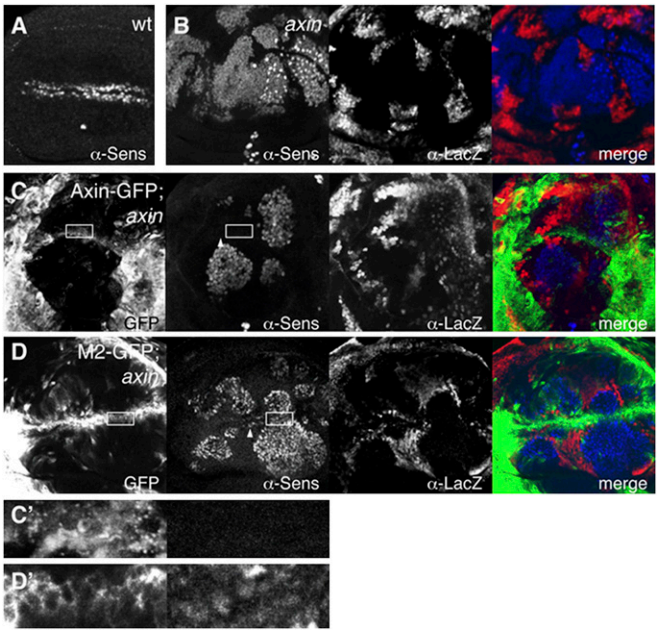

Fig. 3. Polymerization-blocking DAX mutations attenuate Axin's effector function in reducing Wg target gene expression in *axin* null mutant wing disk clones. Fixed wing discs from third instar *Drosophila* larva, stained with α-Sens antibody (*A*), to visualize the Armadillo-dependent expression of this Wg target gene on either side of Wg along the prospective wing margin, double-stained as indicated (*B*), to reveal ectopic Sens (blue) in *axin* null mutant tissue (absence of red, α-lacZ staining), expressing wt or M2 mutant Axin-GFP (green) as indicated (*C* and *D*). (*C′* and *D′*) Boxed areas are at high magnification, revealing that M2 fails to reduce Sens in this *axin* mutant clone (*D′*, *Right*).

observe any chemical shift perturbations if we incubated ^{15}N-DAX_M3 with unlabeled DAX_M3 (Fig. 4*A*) or with the equivalent DIX head mutant (DIX_M4; Fig. S3), as can be seen in the spectral overlays, confirming our MALLS data that the M3 mutations in DAX_M3 block its interactions very effectively.

Interestingly, if we incubate ^{15}N-DAX_M3 with the unlabeled tail mutant DIX_M2, we observe numerous cases of substantial line broadening in addition to chemical shift perturbations of some of the peaks (Fig. 4*B*), demonstrating that the minimal DIX and DAX domains themselves interact directly with one another. To map the DIX-interacting residues in ^{15}N-DAX_M3, we plotted all cases of line broadenings (red) against the DAX residues (Fig. 4*C*), which reveals an excellent correlation between the main DIX-interacting residues of ^{15}N-DAX_M3 (red) with the DAX tail residues in the DAX–DAX polymerization interface (Fig. 1 *A* and *B*), as can be visualized by projecting these line broadenings onto the DAX crystal structure (red; Fig. 5 *A*–*C*). Notably, the head surface of ^{15}N-DAX_M3 does not show any significant shift perturbations, nor any line broadening (Figs. 4*C* and 5 *A* and *B*), as expected because the M3 mutations block the interactions by this surface (see Figs. 1*C* and 4*A*).

We confirmed that the reverse is also true by identifying the DAX_M3-interacting residues within an assigned HSQC spectrum of ^{15}N-DIX_M2 (Fig. S4). In this case, the tail surface of ^{15}N-DIX_M2 is mutant; accordingly, all of the main DAX-interacting residues of ^{15}N-DIX_M2, as detected by NMR (Fig. S5), are clustered in its head surface, as can be visualized if these are projected onto the equivalent residues in the DAX crystal structure (Fig. 5 *D*–*F*). Using NMR titration, we estimate that the heterotypic DIX–DAX interaction (based on incubating ^{15}N-DAX_M3 with different concentrations of DIX_M2) exhibits a lower affinity (200 ± 90 μM) than the homotypic DIX-DIX interaction (5–20 μM; ref. 20). We conclude that the same DAX residues that engage in DAX homopolymerization also mediate a heterotypic interaction with DIX. Indeed, the spectral overlay of ^{15}N-DAX_M3 probed with DIX_M2 versus ^{15}N-DAX_M3 probed with DAX_M5 displays relatively few differences (Fig. S6), providing strong support for the notion that the heterotypic DIX–DAX interaction closely mimics the homotypic DAX–DAX interaction.

Discussion

We have shown that Axin depends critically on DAX-dependent polymerization for its efficient effector function in down-regulating β-catenin in human cells and antagonizing functional

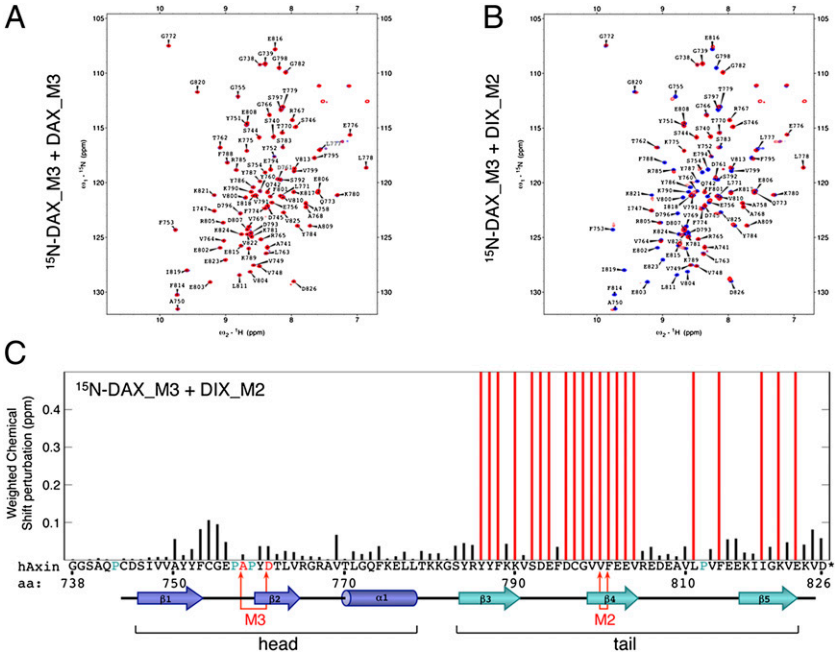

Fig. 4. NMR spectroscopy reveals direct interaction between the polymerization surfaces of DIX and DAX. (*A* and *B*) Overlays of HSQC spectra of 100 μM ^{15}N-DAX_M3 (red) plus 125 μM of unlabeled DAX_M3 (*A*) or DIX_M2 (blue) (*B*), with assigned DAX residues annotated. Numerous line broadenings in *B* signify direct interaction between the head surface of DIX_M2 and the tail surface of ^{15}N-DAX_M3; no perturbations are detectable if the latter is probed with head-surface mutants DAX_M3 (*A*) or DIX_M4 (Fig. S3). (*C*) Shift perturbation map, indicating shifting (black) or line broadening (red) of DAX domain residues (Axin DAX sequence underneath, with symbols as in Fig. 1*A*; turquoise, undetectable prolines).

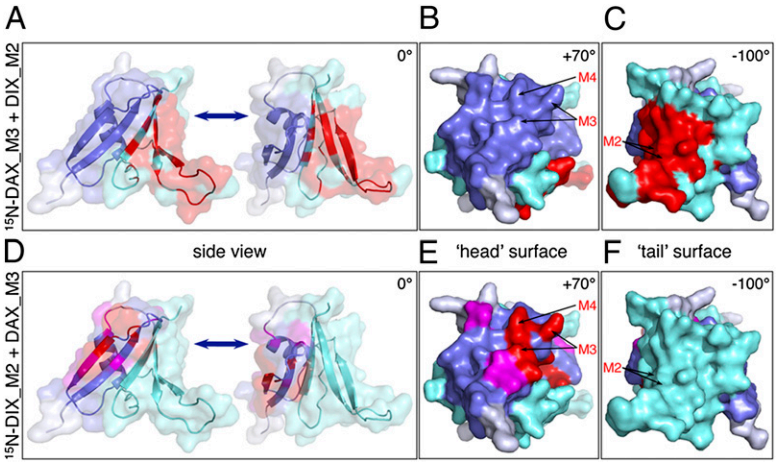

Fig. 5. Projections of the key head and tail interactions between DIX and DAX onto the DAX crystal structure. (*A* and *D*) Ribbon representations of two adjacent DAX monomers (translated apart), with head in blue, and tail in turquoise (Fig. 1 *A* and *B*); DIX-interacting residues are colored in red (line broadening) or magenta (highly significant shifts), based on maps in Fig. 4*C* and Fig. S5. Head (*B* and *E*) and tail (*C* and *F*) surface representations of individual DAX monomers (rotated by angles as indicated), colored as in *A* and *D* (with key interacting residues indicated by arrows).

outputs of Wg and Armadillo signaling in *axin* null mutant *Drosophila* tissues. Importantly, our evidence depends crucially on the use of biochemically well-defined point mutations in the DAX domain that block its self-association in vitro without disturbing the overall protein fold, but also on judicious limiting of the Axin expression levels in all our functional assays. We suggest that the functional dependence of Axin on its DAX domain may have been underestimated in previous tests (e.g., refs. 18 and 28), possibly because these tests involved relatively high expression levels. Our results are entirely consistent with an early study that uncovered a dependence of Axin's effector function in colorectal cancer cells on its DAX domain (13), and we extend this study by demonstrating that the key functional activity of this Axin domain is its ability to polymerize.

We have proposed that the dynamic DIX-dependent polymerization of Dvl2 enables its signaling function by generating a high local concentration of ligand-binding sites, thereby increasing the avidity of Dvl2 for its low-affinity ligands (20). We believe that the same underlying principle also applies to the DAX-dependent polymerization of Axin: Considering its exceedingly low cellular concentration (0.02 nM in *Xenopus* embryos; ref. 29), monomeric Axin would not be expected to bind to its key ligands GSK3β and β-catenin given its relatively low affinities for these proteins [3.2 μM for GSK3β (30); 1.3 nM for β-catenin (31)—too low for an efficient interaction with Axin given that the cellular concentration of unphosphorylated β-catenin is thought to be exceedingly low in the absence of Wnt (29)]. However, the DAX-mediated polymerization of Axin would increase its local cytoplasmic concentration by several orders of magnitude and, thus, enhance its avidity for GSK3β and β-catenin considerably, enabling it to bind efficiently to both enzyme and its substrate. Alternatively, it is also conceivable that the β-catenin destruction complex contains multiple Axin subunits, which could be generated by DAX-dependent multimerization, but we consider this suggestion less likely, given that the above-described head-to-tail polymerization mode does not produce multimers of a defined stoichiometry.

Our NMR analysis demonstrates direct and specific binding between minimal DIX and DAX domains and revealed that the same head and tail residues of the DAX domain that mediate its homopolymerization in the crystal structure (20) also engage in heterotypic interactions with the corresponding head and tail residues of the Dvl DIX domain. Furthermore, our functional assays indicate that the same residues are not only required for Axin's effector function, but also for its response to Dvl/Dsh [refining previous evidence implicating the DAX domain of Axin as the target for inactivation by Dvl (16, 17) and Wg (18)]. Our results have an interesting implication regarding the mechanism how Dvl proteins mediate signaling: In addition to using their DIX domains to stimulate LRP6 phosphorylation and signalosome assembly (6–8) to inhibit GSK3β (9, 10), they could also use this domain to interfere with the effector function of Axin by competing with Axin's polymerization (Fig. S7). According to this model, the dynamic Dvl polymers that form in response to Wnt stimulation at the PM acquire the binding avidity necessary for breaking up the relatively stable Axin assemblies in the cytoplasm, thus mobilizing Axin monomers and copolymerize them into more dynamic Dvl signalsomes (22). This process may involve a relatively slow mechanism of "amalgamation" of the two proteins, as suggested by the observed slow rates of Dvl-dependent recruitment of Axin to the PM (30–60 min; ref. 6), which contrasts with the much faster PM recruitment events reported in other signaling pathways that are due to distinct mechanisms based on direct binding of signal transducers to their membrane receptors (e.g., ref. 32). In summary, by virtue of its DIX domain, Dvl has the potential to behave as a natural dominant-negative of Axin—likely a potent one because its cellular abundance has been estimated to be ≈5,000× in excess of Axin (29). This dominant-negative activity could act in parallel to (and possibly synergize with) Dvl's activity toward LRP6 phosphorylation, which results in direct inhibition of GSK3β (9, 10) and, thus, contribute to a two-pronged signaling activity of Dvl.

For technical reasons, we have not been able to estimate the auto-affinity of DAX, which is likely to be in the mid- to high-micromolar range, like the affinities of DIX–DIX and DIX–DAX, given the similarities of these molecular interactions. This notion implies that the DAX-dependent Axin polymerization, rather than occurring spontaneously and unaided, may require an initiating trigger. We have proposed that the DIX-dependent polymerization of Dvl might be triggered, or stimulated, by Wnt-induced dimerization or clustering of the Fz receptor with its LRP6 coreceptor (6) (Fig. S7). Notably, forced dimerization of polymerization-attenuated DIX mutants can restore signaling activity of Dvl2 (20) and effector function of DAX-less Axin in colorectal cancer cells (13). Axin may thus rely on an as yet unidentified cofactor, present at high cellular concentration and with high affinity to Axin, which would allow it to trigger DAX-dependent Axin dimerization and/or polymerization.

Materials and Methods

Plasmids. The plasmids used were as follows: human HA-Axin-GFP, Flag-Axin, GFP-Dvl2 (21, 22); *Drosophila* Axin-GFP (5); Flag-β-catenin. Human Axin DAX (amino acids 773–862; AAK61224) and Dvl2 DIX (amino acids 1–107) were subcloned into a 6xHis expression vector (pETM-11, EMBL), and M2–M5 mutations were generated by standard QuikChange mutagenesis. All plasmids were verified by sequencing.

Drosophila Strains and Analysis. GFP-tagged M2, M3, and M4 mutants of *Drosophila* Axin (AAD24886) were subcloned into pUAST, and multiple independent transformants were isolated by standard procedures, from which two lines were selected for analysis, based on expression levels (Fig. 2*I*). Other strains used were as follows: *UAS.Axin-GFP*, *arm.GAL4*, *Antp.GAL4* (5); *axin* (24). Mutant germ-line clones were generated by standard procedures, and Axin-expressing *axin* null mutant embryos were selected from the progeny of the cross *hs-flp/+*; *arm.GAL4/+*; *FRT82B axin/FRT82B ovo^D* (or *hs-flp/Antp.GAL4*; *FRT82B axin/FRT82B ovo^D*) × *UAS.Axin-GFP*; *FRT82B axin/Cyo-TM6* on the basis of GFP expression (the compound chromosome *Cyo-TM6* ensures that all GFP-positive embryos are also null mutant for *axin*). For the rescue assays in Fig. 2 *E–G*, embryos were aged at 15 °C to keep Axin expression levels low. Fixation and antibody staining against Wg and En (Developmental Studies Hybridoma Bank), Armadillo (33), and GFP (with chicken α-GFP; Abcam) were done as described (5). Cuticles were prepared by standard procedures. *axin* wing disk clones were generated with *vg.GAL4 UAS.flp* (34), and paraformaldehyde-fixed discs were stained with α-Sens (35) and α-β-galactosidase (Promega) as described (25).

Functional Assays in Human Cells. Cells were grown in DMEM, supplemented with 10% FBS, and transfected in six-well plates with Lipofectamine 2000 (Invitrogen). To keep Axin expression levels low, 100 ng per well of Axin expression vectors were used for all transfections (supplemented with pRL-TK plasmid to 500 ng per well), except for Fig. 1 *D* and *E* (6, 22). Fixation and staining with mouse α-β-catenin (Transduction Laboratories) was done as described (22). Mouse and rabbit α-Flag, mouse α-tubulin, and α-actin (Sigma) were also used. For Western blots, mouse α-ABC (8E7, Millipore) and rat α-HA (3F10, Roche) were used.

Protein Purification. DIX and DAX proteins were expressed in BL21(DE3)-RIL and purified with Ni-NTA resin, followed by gel filtration.

NMR Spectroscopy. Protein expression was done in minimal medium supplemented by ^{15}N-ammonium chloride and ^{13}C-glucose, purified as above followed by proteolytic removal of His tag. NMR spectra were recorded with a Bruker Avance spectrometer at 800 MHz ^{1}H, with a triple resonance inverse cryogenic probehead (sample temperature 25 °C). Samples contained 100 μM ^{13}C/^{15}N-labeled DAX or DIX, with or without 125 μM unlabeled binding partner, in 25 mM phosphate buffer (pH 6.8, 150 mM sodium chloride, 5% vol/vol ^2H_2O). Backbone resonance assignments were obtained by standard triple resonance techniques [HNCACB, CBCA(CO)NH, HNCO, and HN(CA)CO]. For chemical-shift mapping, a fast-HSQC spectrum (36) was obtained with 1,024 and 256 data points in t_2 and t_1, respectively, with spectral widths of 11,061 and 2,756 Hz. The number of points in t_1 was doubled by forward complex linear prediction before Fourier transformation. Spectra were processed with TopSpin version 2 (Bruker) and analyzed with Sparky version 3.110 (Goddard & Kneller). For DIX-DAX affinity estimates, 100 μM ^{15}N-DAX_M3 was titrated with increasing amounts (25, 50, 75, 125, and 200 μM) of unlabeled DIX_M2.

MALLS. Purified His-DIX and His-DAX were subjected to size exclusion chromatography/MALLS with an ÄKTA FPLC Chromatographic system (GE Healthcare) connected to a Dawn Heleos II 18-angle light scattering detector combined with an Optilab rEX differential refractometer (Wyatt). Samples were loaded onto a Superdex-75 HR10/30 gel filtration column (GE Healthcare) at 2 mg/mL and run at 0.5 mL/min in buffer (20 mM Tris at pH 7.4, 200 mM NaCl, and 0.01% NaN_3). Data were processed with Astra V software.

ACKNOWLEDGMENTS. We thank Marc de la Roche and Hugo Bellen for antibodies, Olga Perisic for technical advice, and Tom Miller and Stefan Freund for discussions. This work was supported by Cancer Research UK Grant C7379/A8709 (to M.B.) and Medical Research Council Grant U105103 0200000101.

1. Clevers H (2006) Wnt/β-catenin signaling in development and disease. *Cell* 127: 469–480.
2. MacDonald BT, Tamai K, He X (2009) Wnt/β-catenin signaling: Components, mechanisms, and diseases. *Dev Cell* 17:9–26.
3. Ikeda S, et al. (1998) Axin, a negative regulator of the Wnt signaling pathway, forms a complex with GSK-3β and β-catenin and promotes GSK-3β-dependent phosphorylation of β-catenin. *EMBO J* 17:1371–1384.
4. Dajani R, et al. (2003) Structural basis for recruitment of glycogen synthase kinase 3β to the axin-APC scaffold complex. *EMBO J* 22:494–501.
5. Cliffe A, Hamada F, Bienz M (2003) A role of Dishevelled in relocating Axin to the plasma membrane during wingless signaling. *Curr Biol* 13:960–966.
6. Bilic J, et al. (2007) Wnt induces LRP6 signalosomes and promotes dishevelled-dependent LRP6 phosphorylation. *Science* 316:1619–1622.
7. Zeng X, et al. (2008) Initiation of Wnt signaling: Control of Wnt coreceptor Lrp6 phosphorylation/activation via frizzled, dishevelled and axin functions. *Development* 135:367–375.
8. Metcalfe C, Mendoza-Topaz C, Mieszczanek J, Bienz M (2010) Stability elements in the LRP6 cytoplasmic tail confer efficient signalling upon DIX-dependent polymerization. *J Cell Sci* 123:1588–1599.
9. Piao S, et al. (2008) Direct inhibition of GSK3β by the phosphorylated cytoplasmic domain of LRP6 in Wnt/β-catenin signaling. *PLoS ONE* 3:e4046.
10. Wu G, Huang H, Garcia Abreu J, He X (2009) Inhibition of GSK3 phosphorylation of β-catenin via phosphorylated PPPSPXS motifs of Wnt coreceptor LRP6. *PLoS ONE* 4: e4926.
11. Behrens J, et al. (1998) Functional interaction of an axin homolog, conductin, with β-catenin, APC, and GSK3β. *Science* 280:596–599.
12. Hart MJ, de los Santos R, Albert IN, Rubinfeld B, Polakis P (1998) Downregulation of β-catenin by human Axin and its association with the APC tumor suppressor, β-catenin and GSK3 β. *Curr Biol* 8:573–581.
13. Sakanaka C, Williams LT (1999) Functional domains of axin. Importance of the C terminus as an oligomerization domain. *J Biol Chem* 274:14090–14093.
14. Hsu W, Zeng L, Costantini F (1999) Identification of a domain of Axin that binds to the serine/threonine protein phosphatase 2A and a self-binding domain. *J Biol Chem* 274: 3439–3445.
15. Luo W, et al. (2005) Axin contains three separable domains that confer intramolecular, homodimeric, and heterodimeric interactions involved in distinct functions. *J Biol Chem* 280:5054–5060.
16. Kishida S, et al. (1999) DIX domains of Dvl and axin are necessary for protein interactions and their ability to regulate β-catenin stability. *Mol Cell Biol* 19: 4414–4422.
17. Smalley MJ, et al. (1999) Interaction of axin and Dvl-2 proteins regulates Dvl-2-stimulated TCF-dependent transcription. *EMBO J* 18:2823–2835.
18. Peterson-Nedry W, et al. (2008) Unexpectedly robust assembly of the Axin destruction complex regulates Wnt/Wg signaling in Drosophila as revealed by analysis in vivo. *Dev Biol* 320:226–241.
19. Wong CK, et al. (2004) The DIX domain protein coiled-coil-DIX1 inhibits c-Jun N-terminal kinase activation by Axin and dishevelled through distinct mechanisms. *J Biol Chem* 279:39366–39373.
20. Schwarz-Romond T, et al. (2007) The DIX domain of Dishevelled confers Wnt signaling by dynamic polymerization. *Nat Struct Mol Biol* 14:484–492.
21. Schwarz-Romond T, Merrifield C, Nichols BJ, Bienz M (2005) The Wnt signalling effector Dishevelled forms dynamic protein assemblies rather than stable associations with cytoplasmic vesicles. *J Cell Sci* 118:5269–5277.
22. Schwarz-Romond T, Metcalfe C, Bienz M (2007) Dynamic recruitment of axin by Dishevelled protein assemblies. *J Cell Sci* 120:2402–2412.
23. Morin PJ, et al. (1997) Activation of β-catenin-Tcf signaling in colon cancer by mutations in β-catenin or APC. *Science* 275:1787–1790.
24. Hamada F, et al. (1999) Negative regulation of Wingless signaling by D-axin, a Drosophila homolog of axin. *Science* 283:1739–1742.
25. Parker DS, Jemison J, Cadigan KM (2002) Pygopus, a nuclear PHD-finger protein required for Wingless signaling in Drosophila. *Development* 129:2565–2576.
26. Choi SH, Choi KM, Ahn HJ (2010) Coexpression and protein-protein complexing of DIX domains of human Dvl1 and Axin1 protein. *BMB Rep* 43:609–613.
27. Capelluto DG, et al. (2002) The DIX domain targets dishevelled to actin stress fibres and vesicular membranes. *Nature* 419:726–729.
28. Itoh K, Krupnik VE, Sokol SY (1998) Axis determination in Xenopus involves biochemical interactions of axin, glycogen synthase kinase 3 and β-catenin. *Curr Biol* 8:591–594.
29. Lee E, Salic A, Krüger R, Heinrich R, Kirschner MW (2003) The roles of APC and Axin derived from experimental and theoretical analysis of the Wnt pathway. *PLoS Biol* 1:E10.
30. Bax B, et al. (2001) The structure of phosphorylated GSK-3β complexed with a peptide, FRATtide, that inhibits β-catenin phosphorylation. *Structure* 9:1143–1152.
31. Choi HJ, Huber AH, Weis WI (2006) Thermodynamics of β-catenin-ligand interactions: The roles of the N- and C-terminal tails in modulating binding affinity. *J Biol Chem* 281:1027–1038.
32. Hsieh MY, Yang S, Raymond-Stinz MA, Edwards JS, Wilson BS (2010) Spatio-temporal modeling of signaling protein recruitment to EGFR. *BMC Syst Biol* 4:57.
33. de la Roche M, Bienz M (2007) Wingless-independent association of Pygopus with dTCF target genes. *Curr Biol* 17:556–561.
34. Végh M, Basler K (2003) A genetic screen for hedgehog targets involved in the maintenance of the Drosophila anteroposterior compartment boundary. *Genetics* 163:1427–1438.
35. Nolo R, Abbott LA, Bellen HJ (2000) Senseless, a Zn finger transcription factor, is necessary and sufficient for sensory organ development in Drosophila. *Cell* 102: 349–362.
36. Mori S, Abeygunawardana C, Johnson MO, van Zijl PC (1995) Improved sensitivity of HSQC spectra of exchanging protons at short interscan delays using a new fast HSQC (FHSQC) detection scheme that avoids water saturation. *J Magn Reson B* 108:94–98.